Nontrivial interface states confined between two topological insulators

Tomáš Rauch,[1] Markus Flieger,[1] Jürgen Henk,[1] and Ingrid Mertig[1,2]
[1]*Institut für Physik, Martin-Luther-Universität Halle-Wittenberg, D-06099 Halle (Saale), Germany*
[2]*Max-Planck-Institut für Mikrostrukturphysik, D-06120 Halle (Saale), Germany*
(Received 19 July 2013; revised manuscript received 25 October 2013; published 17 December 2013)

By *ab initio* based tight-binding calculations, we show that nontrivial electronic states exist at an interface of a $\mathcal{Z}_2$ topological insulator and a topological crystalline insulator. At the exemplary (111) interface between Bi_2Te_3 and SnTe, the two Dirac surface states at the Brillouin zone center $\overline{\Gamma}$ annihilate upon approaching the semi-infinite subsystems but one topologically protected Dirac surface state remains at each time-reversal invariant momentum $\overline{M}$. This leads to a highly conducting spin-momentum-locked channel at the interface but insulating bulk regions. For the Sb_2Te_3/Bi_2Te_3 interface, we find complete annihilation of Dirac states because both subsystems belong to the same topology class. Our proof of principle may have impact on planar electric transport in future spintronics devices with topologically protected conducting channels.

DOI: 10.1103/PhysRevB.88.245120 PACS number(s): 73.20.At, 71.70.Ej

I. INTRODUCTION

Three-dimensional topological insulators are a new class of materials that are characterized by an insulating bulk but highly conducting surface states.[1] These surface states bridge the fundamental band gap and are topologically protected against perturbations. Two classes of three-dimensional topological insulators (TIs) are currently investigated with great effort: $\mathcal{Z}_2$ TIs rely on time-reversal symmetry and an odd number of band inversions in the bulk Brillouin zone; topological crystalline insulators (TCIs)[2] require a crystal symmetry, in particular, mirror symmetry, but may possess an even number of band inversions. Brought about by the spin-orbit interaction, the fundamental band gaps of TIs are small compared to those of typical band insulators (100–250 meV).

Prominent examples for $\mathcal{Z}_2$ TIs are the chalcogenides Bi_2Se_3, Bi_2Te_3, and Sb_2Te_3, each showing a band inversion at the center Γ of the bulk Brillouin zone. They are characterized by $\mathcal{Z}_2$ topological invariants $(\nu_0;\nu_1\,\nu_2\,\nu_3) = (1;0\,0\,0)$ (see Ref. 3) and have a single Dirac surface state at the center $\overline{\Gamma}$ of their (111) surface's Brillouin zone. The spin chirality of these surface states is dictated by those p orbitals that make up the inverted band gap; thus, it is identical among the chalcogenides.[4–6] As a consequence, the two Dirac surface states at a common interface of two chalcogenide TIs annihilate because the two subsystems are in the same topological phase. They would not annihilate if their spin chirality would be opposite;[7] however, such a $\mathcal{Z}_2$ TI is yet unknown.

One representative of a TCI with mirror symmetry is SnTe,[8,9] showing band inversions at the L points of the bulk Brillouin zone. For a mirror plane that is spanned by four L points, the relevant topological invariant—the mirror Chern number—equals -2. Thus there are two Dirac points associated with that plane. For the (001) surface, these are close to the time-reversal invariant momentum (TRIM) $\overline{X}$. This crystal orientation does not fit to the commonly investigated (111) orientation of the chalcogenides which is naturally induced by their quintuple-layer geometry. Therefore, to form a common interface of SnTe and Bi_2Te_3, one should choose the (111) surface of SnTe that also shows two Dirac surface states, one at $\overline{\Gamma}$ (as, e. g., Bi_2Te_3), another at $\overline{M}$; these states have identical spin chirality. Because the chalcogenides are also topological crystalline insulators, with a mirror Chern number of -1 (see Ref. 10), the spin chiralities of the surface states of SnTe and Bi_2Te_3 are identical as well. As a consequence, surface states annihilate at a common interface of SnTe and Bi_2Te_3.

From these considerations, the question arises whether all Dirac surface states of Bi_2Te_3(111) and SnTe(111) annihilate at a common interface. Or do only two of them obliterate each other and does one nontrivial surface state remain (see Fig. 1)? In this Paper, we provide a proof of principle by means of *ab initio* based tight-binding calculations that the pair of Dirac surface states at $\overline{\Gamma}$ indeed annihilates but the Dirac surface state at $\overline{M}$ "survives." This remaining electronic state is topologically protected by mirror symmetry and results in a highly conducting channel at the interface of two bulk topological insulators. This conductance channel with spin-momentum locking could be utilized in future electronics. For comparison, the Sb_2Te_3/Bi_2Te_3 interface shows complete annihilation of Dirac states because both subsystems belong to the same topology class, resulting in an entirely insulating system.

The paper is organized as follows. Theoretical aspects are addressed in Sec. II, in which we provide details of the electronic structure calculations (Sec. II A) and topological-invariant calculations (Sec. II B). Results are discussed in Sec. III. For the topological heterophase system $SnTe/Bi_2Te_3$, we address the annihilation and survival of the Dirac states (Sec. III A 1), a model Hamiltonian (Sec. III A 2), and the localization of the Dirac states (Sec. III A 3). The complete annihilation of Dirac states in the topological iso-phase system Sb_2Te_3/Bi_2Te_3 is presented in Sec. III B. A sum rule for the number of Dirac states at an interface is given in Sec. III C, before concluding with Sec. IV.

II. THEORETICAL ASPECTS

A. Tight-binding calculations

The purpose of our approach is to support our main statement of annihilation of a pair of Dirac states and the survival of one Dirac state. To do so, the method accounts for

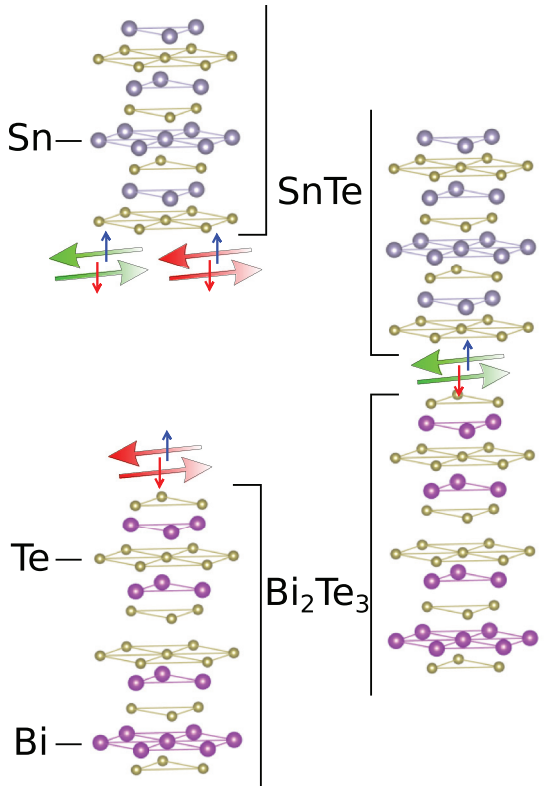

FIG. 1. (Color online) Topologically nontrivial electronic states at the (111) surfaces of the $\mathcal{Z}_2$ topological insulator Bi_2Te_3 and the topological crystalline insulator SnTe (left) as well at their common interface (right). Bi_2Te_3(111) hosts one state (red arrows), while SnTe(111) hosts two states (red and green arrows). Upon formation of an interface, the "red" surface states annihilate but the "green" SnTe-derived state survives. Spin and momentum are locked: states propagating to the left are spin up (small blue arrows), states propagating to the right are spin down (small red arrows). Te, Bi, and Sn atoms are displayed in brown, magenta, and grey, respectively.

the correct boundary conditions of an interface[48] and relies on a tight-binding parametrization, which works also well for other chalcogenides and rocksalt insulators.[11]

The empirical tight-binding method interpolates the band structure that has been determined by advanced first-principles methods. We adopted Slater-Koster parameters, from Ref. 12 for Bi_2Te_3 as well as from Ref. 13 for SnTe. The parameters for Sb_2Te_3 have been fitted to an *ab initio* band structure using a Monte Carlo method.[14,15] Spin-orbit coupling is treated as in Ref. 16. All parameter sets yield good agreement, in particular for the important energy range near the fundamental band gap.[17]

The resulting band structures were checked against our first-principles Korringa-Kohn-Rostoker, VASP, and WIEN2K calculations.[11,18–20] The agreement puts our tight-binding approach on a firm and reliable basis. The bulk bands are obtained by diagonalization of the Hamilton operator matrix in the basis of Bloch states $\Phi_\alpha(\vec{k})$, with α a compound index of orbital, spin orientation, and atom; $\vec{k}$ is the wave vector.

The electronic structures of the (111) surfaces and interfaces have been obtained for the semi-infinite systems, using a renormalization scheme for the Green function, originally developed for surfaces[21,22] and later extended to interfaces.[23] A description of this scheme is rather lengthy; therefore we provide a sketch here. The system is decomposed into principal layers in such a way that only adjacent principal layers interact, making the Hamiltonian matrix H block-tridiagonal. These interactions are reduced by a renormalization process using the defining matrix equation

$$\mathsf{G}(z,\vec{k}_\parallel)[z\mathsf{1} - \mathsf{H}(\vec{k}_\parallel)] = \mathsf{1}, \tag{1}$$

in which $z = E + i\eta$, $\eta > 0$, is a complex energy argument. For vanishing interlayer interaction, this scheme yields layer-resolved blocks $\mathsf{G}_{lm}(z,\vec{k}_\parallel)$ of the Green function matrix which is indexed by compound indices α and β (l and m principal layer indices; $\vec{k}_\parallel$ surface-parallel wave vector). Surface and interface states appear "naturally" in this procedure, e. g., without additional treatment.[24]

The layer-resolved spectral density is then computed from

$$N_l(E,\vec{k}_\parallel) = -\frac{1}{\pi}\lim_{\eta\to 0^+} \mathrm{Im}\ \mathrm{tr}_\alpha\ \mathsf{G}_{ll}(E+i\eta,\vec{k}_\parallel). \tag{2}$$

Appropriate partial traces allow to decompose the spectral density with respect to, e. g., spin projection and orbital.

The spin texture of the Dirac states is investigated by means of spin-resolved spectral densities, with spin projections typically along the Cartesian axes. Instead of the spin polarization, we use spin differences:

$$\vec{S}_l(E,\vec{k}_\parallel) = -\frac{1}{\pi}\lim_{\eta\to 0^+} \mathrm{Im}\ \mathrm{tr}_\alpha\ [\vec{\sigma}\mathsf{G}_{ll}(E+i\eta,\vec{k}_\parallel)], \tag{3}$$

where $\vec{\sigma}$ is the vector of Pauli matrices. The limit $\eta \to 0^+$ in Eqs. (2) and (3) is not taken but typically $\eta = 2$ meV.

The dispersions of the Dirac states show up as maxima in $N_{\alpha l}(E,\vec{k}_\parallel)$ of the interface layers; they agree well with those obtained from our first-principles Korringa-Kohn-Rostoker (semi-infinite system) and VASP (slab of at least six quintuple layers) calculations for Bi_2Te_3 and Sb_2Te_3. For SnTe, we checked also the electronic structure of the (001) surface and found agreement with that reported in Ref. 8.

The lattice constants of Bi_2Te_3 and SnTe show a mismatch of about 2 %. We assume that SnTe(111) adopts the in-plane lattice constant of Bi_2Te_3; the out-of-plane (interlayer) distance is chosen to conserve the volume of the bulk unit cell. The tight-binding parameters of SnTe have, thus, been scaled using Harrison's d^{-2} law.[25] SnTe remains a topological crystalline insulator in this distorted phase but with a reduced width of the fundamental band gap (250 meV $\to$ 40 meV). Although the Slater-Koster parameters at the surface or interface are taken from bulk values, the surface electronic structures agree with those reported earlier.[8,19] The valence band maxima of the bulk systems have been aligned to the common Fermi level in the interface system, in accordance with the "common anion rule" (see Ref. 26).

Concerning the SnTe/Bi_2Te_3 interface, the outermost SnTe layer is made of Te atoms.[49] The distance between these atoms and the outermost Te atoms of Bi_2Te_3 is assumed identical to that between the outermost Te atoms of adjacent quintuple layers of Bi_2Te_3 (i. e., the van der Waals gap). Therefore the Slater-Koster parameters at the interface are identical to

those describing the coupling between two quintuple layers of Bi_2Te_3.

To perform the transition from two separate surfaces to a joint interface, we scale the tight-binding parameters that mediate the hopping between the two half-spaces by a factor κ, with $\kappa = 0$ ($\kappa = 1$) for zero (full) coupling; confer the bond-cutting mechanism in Ref. 27. This procedure can be viewed as letting the surfaces approach in real space (schematically shown Fig. 1): $\kappa = 0$ mimics an infinite distance. NB: we could have used Harrison's d^{-2} scaling (see Ref. 25), with identical results for the most important cases: vanishing and full coupling.

The tight-binding parameters of the surface or interface layers were not changed with respect to those of the bulk. The (111) surfaces of both the chalcogenides and SnTe show band bending due to their polar nature. For Bi_2Se_3(111), the band bending region extends about 200 Å (see Ref. 28), and we expect a similar width for Bi_2Te_3. Because the Dirac surface state is strongly located in the first quintuple layer (see below) it is mildly affected by the band bending. In the *ab initio* calculations reported in Ref. 19, in which the potentials of the first five quintuple layers are allowed to differ from those in the bulk, no clear indication for band bending was found. Although these two findings seem to contradict each other, they both support to neglect the band bending in the description of the Dirac surface state of Bi_2Te_3 for the time being.

Concerning SnTe, an appropriate *ab initio* description requires advanced exchange-correlation functionals, e. g., hybrid functionals[11] [the self-consistent calculation for SnTe(001) reported in Ref. 8 relies on the generalized gradient approximation]. This makes such advanced density-functional calculations computationally very demanding for the bulk system but nearly impossible for a surface system. Our tight-binding approach is numerically much less demanding and, importantly, it reproduces very well the bulk electronic structure of Ref. 11 and the Dirac surface states of SnTe(001) reported in Refs. 8 and 9.

Hybrid functionals give a better description of the fundamental band gap than the often used local density approximation for the exchange-correlation functional. This is in particular important for small-gap semiconductors (here, SnTe). A too small band gap would result in a distorted dispersion relation of the topologically protected surface states.

Being computationally demanding, a hybrid-functional calculation mimicking a surface system might be performed for a slab with small thickness. Therefore surface states located at either side of the slab would hybridize and show artificial band gaps due to quantum confinement. These gaps could be significantly wide for weakly localized surfaces states, as would be the case for the surface state in SnTe(111) at $\overline{M}$, as we will see below. In our study on Bi_2Te_3/SnTe interfaces, the opening up of band gaps is a crucial point; artificial band gaps would make the interpretation difficult and, thus, should be avoided. In our approach, this problem is overcome by the renormalization technique for semi-infinite systems.

For the band alignment, we follow the common anion rule (see Refs. 29–31), discussed in the supplement of Ref. 26. This rule applies to interfaces of insulators with a common anion. In this case, the valence electronic states are primarily derived from the anion orbitals (Te) whereas the conduction bands are primarily derived from the cation orbitals. Consequently, the valence states should be similar, leading to a smaller offset of the valence bands than of the conduction bands. Taskin *et al.* argue that the band bending shows up mainly in Bi_2Te_3 rather than in SnTe (see Ref. 26).

B. Calculation of $\mathcal{Z}_2$ invariants and mirror Chern numbers

The tight-binding method allows a fast and reliable computation of topological invariants.[3] The $\mathcal{Z}_2$ invariant is calculated from the Fu-Kane formula[32] discretized according to Fukui and Hatsugai.[33] For sufficiently dense $\vec{k}$ meshes we compute the $\mathcal{Z}_2$ invariants $(\nu_0; \nu_1\,\nu_2\,\nu_3) = (1; 0\,0\,0)$ for Bi_2Te_3 and Sb_2Te_3 as well as $(0; 0\,0\,0)$ for SnTe.

In the calculation of the mirror Chern number, we follow the idea of the spin Chern number.[34] The considered mirror plane is normal to a (11$\bar{1}$) surface plane; in reciprocal space, it comprises the $\overline{\Gamma}$ and $\overline{M}$ points of the surface Brillouin zone (confer Fig. 1 in both Ref. 8 and 10). The Bloch states with wave vector $\vec{k}$ within this mirror plane are eigenstates of both the Hamiltonian and the mirror operator.[35] This allows us to divide the Bloch states into two categories: one with mirror eigenvalue $+\mathrm{i}$, the other with eigenvalue $-\mathrm{i}$. The $\vec{k}$-dependent Berry curvature is calculated for both of them. The weighted sum of the Berry curvature over a discrete $\vec{k}$ set in the intersection of the mirror plane with the Brillouin zone gives the Chern number $n_{\pm\mathrm{i}}$ for each category. The mirror Chern number is then obtained from[4]

$$c_\mathrm{m} \equiv \frac{n_{+\mathrm{i}} - n_{-\mathrm{i}}}{2}. \tag{4}$$

We calculate the mirror Chern number for a mesh of 100×100 k points, getting $c_\mathrm{m} = -1$ for Bi_2Te_3 and Sb_2Te_3 as well as -2 for SnTe, with a relative error less than 10^{-4}.

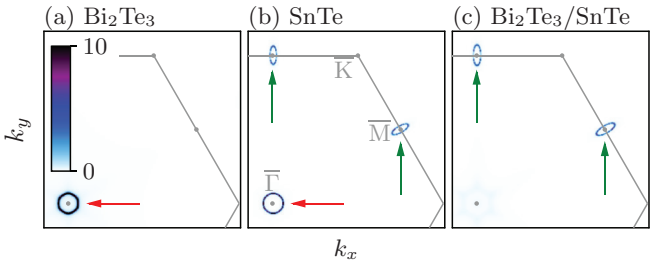

FIG. 2. (Color online) Electronic structure of (a) the Bi_2Te_3(111) surface, (b) the SnTe(111) surface, and (c) a Bi_2Te_3/SnTe(111) interface. The spectral densities of the outermost surface layers [(a) and (b)] or the SnTe interface layer (c) are shown as color scale (in states/eV) for a constant energy of 0.08 eV (i. e., within the fundamental band gap). In each panel, the same part of the hexagonal Brillouin zone is displayed; high-symmetry points and the Brillouin zone edge are indicated by grey dots and lines, respectively. Arrows mark surface and interface states.

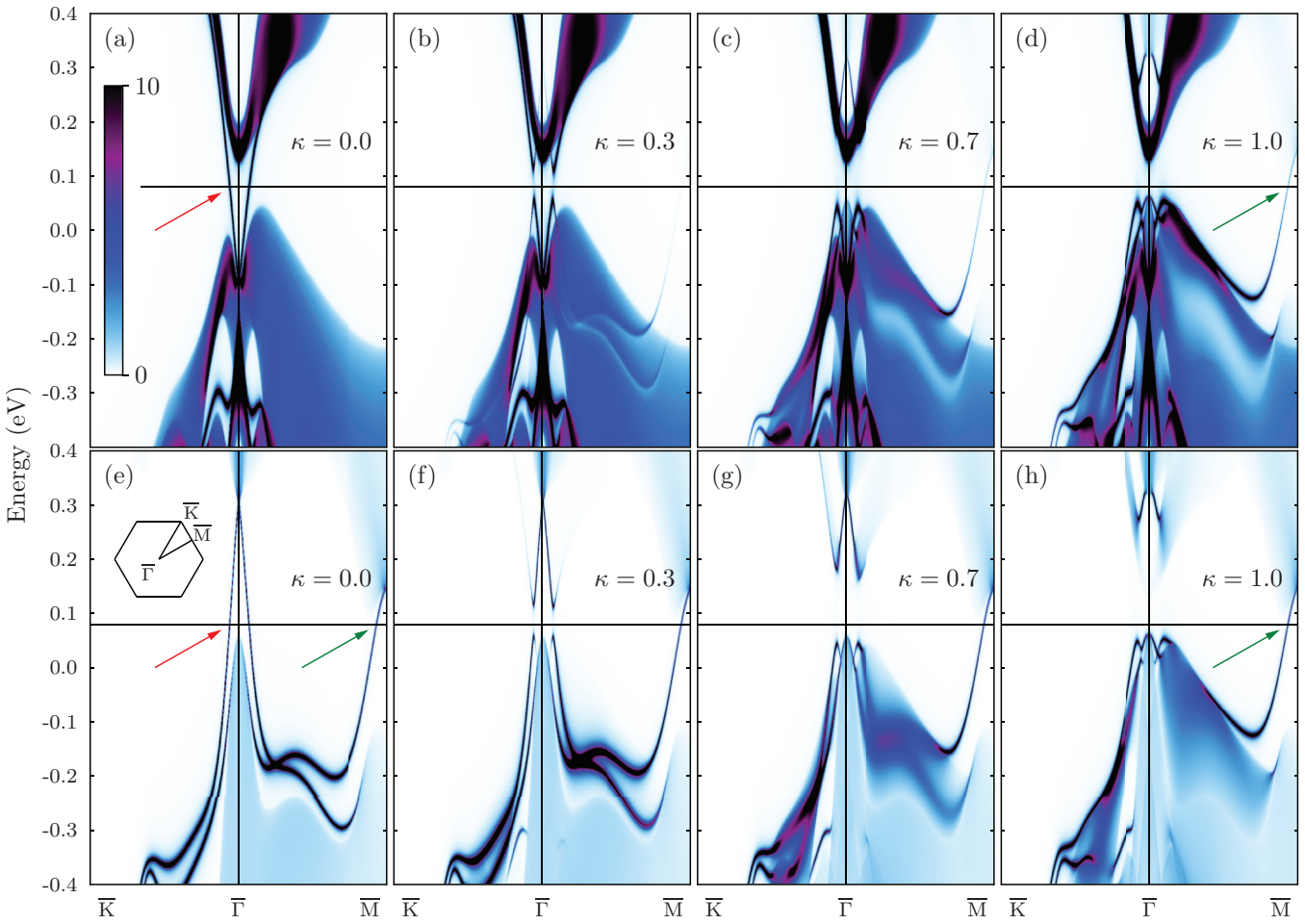

FIG. 3. (Color online) Electronic structure of a Bi_2Te_3/SnTe(111) interface, obtained from tight-binding calculations. The spectral densities of the outermost Bi_2Te_3 [top, (a)–(d)] and SnTe [bottom, (e)–(h)] interface layers are shown as color scale (in units of states/eV) for a $\overline{K}$-$\overline{\Gamma}$-$\overline{M}$ path in the two-dimensional Brillouin zone [inset in (e)]. The coupling strength κ of the semi-infinite systems increases from left to right ($\kappa = 0$ uncoupled; $\kappa = 1$ fully coupled). The horizontal lines mark the energy of 0.08 eV used in Fig. 2. Arrows in (a), (d), (e), and (h) point towards Dirac surface or interface states (also indicated in Fig. 2).

III. DISCUSSION AND RESULTS

A. Interface electronic structure of SnTe(111)/Bi_2Te_3(111)

1. *Annihilation and survival of Dirac states*

The surface band structure of Bi_2Te_3(111) shows the well-known Dirac surface state, with its Dirac point close to the valence bands at $\overline{\Gamma}$. In a constant energy cut (CEC), this state results in a slightly warped[36] circular shape [red arrow in Fig. 2(a)]. The (111) surface of SnTe hosts two Dirac states: the state at $\overline{\Gamma}$ produces a circular shape in a CEC [red arrow in Fig. 2(b)], the equivalent states at $\overline{M}$ show up as ellipses [green arrows in Fig. 2(b)].

Upon approaching the two semi-infinite systems, that is by increasing κ to 1, the two circular contours at $\overline{\Gamma}$ disappear but the structures at $\overline{M}$ remain [green arrows in Fig. 2(c)]. This "annihilation" of the pair of states at $\overline{\Gamma}$ can be interpreted by opening of a band gap in the two respective surface states.

This scenario is illustrated by the interface electronic structure for selected coupling strengths κ (see Fig. 3). For $\kappa = 0$, we find the surface band structures of Bi_2Te_3 and SnTe, both showing a Dirac surface state at $\overline{\Gamma}$ bridging the fundamental band gap (red arrows in a and e). The Dirac points are close

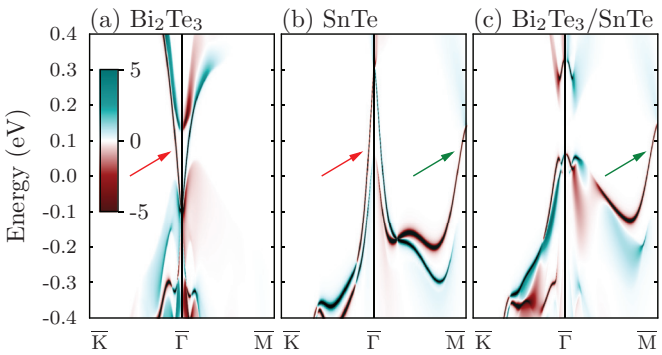

FIG. 4. (Color online) Spin-resolved electronic structure of (a) Bi_2Te_3(111), (b) SnTe(111), and (c) Bi_2Te_3/SnTe(111). The spectral spin differences of the outermost surface layer [(a) and (b); $\kappa = 0$] and the SnTe interface layer [(c), $\kappa = 1$], presented as color scale (in units of states/eV), are resolved with respect to the Rashba component of the spin polarization. Arrows mark Dirac surface or interface states, as in Fig. 3.

to the valence bands, in Bi_2Te_3, or to the conduction bands, in SnTe. With increasing κ, the Bi_2Te_3 layer "picks up" spectral weight from SnTe, seen by the pale colors, and vice versa.

A first important observation is that a band gap opens up in the $\overline{\Gamma}$ surface states because these states have identical spin chirality; compare Figs. 3(a) and 3(b) as well as Figs. 3(e) and 3(f). The width of this band gap increases with κ [Figs. 3(c) and 3(g)], so that for full coupling these surface states merge with the bulk-state continuum and are entirely shifted out of the fundamental band gap [Figs. 3(d) and 3(h)]. The band gap opening is accompanied by the formation of Rashba-type dispersions, clearly seen in Fig. 3(f). Such a dispersion has been observed for surface states in Au(111) and Bi/Ag(111).[37,38] The hybridization of the two Dirac states turns their linear dispersion of massless relativistic Fermions into the spin-orbit-split dispersion of massive electrons.

Another striking feature is that the SnTe surface state at $\overline{M}$ [green arrow in Fig. 3(e)] "survives" the formation of the interface [green arrows in Figs. 3(d) and 3(h)]. More precisely, its dispersion does not change significantly with κ [Figs. 3(e)–3(h)], which is readily explained by the considerable local band gap around $\overline{M}$. It is this Dirac interface state that forms a topologically protected conducting channel in an otherwise insulating system. In contrast, the two Dirac surface states at $\overline{\Gamma}$ in Bi_2Te_3/Sb_2Te_3 annihilate upon increasing the coupling κ because both subsystems are in the same topological phase (see Sec. III B).

In view of applications, the spin textures of the surface and interface states are essential quantities; in particular, spin-momentum locking could be used in spintronics devices.[39] The spin polarization of the $Bi_2Te_3(111)$ Dirac state is of Rashba type: the spin is mostly in-plane and perpendicular to $\vec{k}_\parallel$ [see Fig. 4(a)]; the degree of spin polarization equals 53 %, in agreement with first-principles calculations.[19,40] Along $\overline{K}$-$\overline{\Gamma}$, it is tilted out-of-plane due to warping (not shown here).[19,36]

The $\overline{\Gamma}$ surface state of SnTe(111) shows the same spin chirality as its counterpart in Bi_2Te_3 [see Fig. 4(b)], which is indicated by the identical sign of their mirror Chern number.[50] At the energy of the constant energy cuts of Fig. 2, the spin helicity of all Dirac states is clockwise. Note within this respect that Figs. 4(a) and 4(b) show facing surfaces. The surface states are almost completely spin polarized (93 % close to $\overline{\Gamma}$, 98 % close to $\overline{M}$); the state at $\overline{M}$ displays an out-of-plane component of 15 % on the $\overline{M}$-$\overline{K}$ line.

The spin-momentum locking of the surviving interface state at $\overline{M}$ is proven in Fig. 4(c). In the SnTe interface layer, the Rashba spin polarization is 98 % along $\overline{\Gamma}$-$\overline{M}$; along $\overline{M}$-$\overline{K}$ it equals 90 %, with an out-of-plane contribution of 21 %. In the adjacent Bi_2Te_3 quintuple layer, these numbers are slightly less (77 %, 81 %, and 10 %, respectively). This large degree of spin polarization lends itself support for spintronics applications.

2. Model Hamiltonian

The Dirac states at $\overline{M}$ are well described by the Hamiltonian (in atomic units; $\hbar = m_e = 1$)

$$\widehat{H} = \frac{k_x^2}{2m_x^\star} + \frac{k_y^2}{2m_y^\star} + \alpha_{xy}k_x\sigma_y + \alpha_{yx}k_y\sigma_x + \alpha_{xz}k_x\sigma_z, \quad (5)$$

which has been derived from $\vec{k}\cdot\vec{p}$ theory for the point group C_s (see Refs. 35 and 41). $\vec{k}_\parallel$ is centered at $\overline{M}$, the σ's are Pauli matrices. A fit to the tight-binding bands yields effective masses of $m_x^\star = -0.01$ and $m_y^\star = -0.03$, which indicate almost linear dispersion. The spin-orbit parameters read $\alpha_{xy} = 0.89$ eV Å, $\alpha_{yx} = 3.31$ eV Å, and $\alpha_{xz} = 0.77$ eV Å. The in-plane α's are strongly anisotropic, as expected from the elongated CECs. α_{yx} is even larger than the "giant" Rashba parameter of Bi/Ag(111) (3.05 eV Å, Ref. 38).

3. Surface and interface localization of Dirac states

We investigated the localization of the Dirac states for the uncoupled ($\kappa = 0$) and the fully coupled ($\kappa = 1$) systems. For the surface system SnTe(111), the Dirac surface state with a Dirac point at $\overline{\Gamma}$ is strongly localized at the surface (top row in Fig. 5); this is deduced from the color saturation decreasing from (a) to (c) and almost zero spectral weight in (d) and (e). The other Dirac state, with a Dirac point at $\overline{M}$, is comparably weakly localized at the surface, as seen by the nonzero but small spectral weight in (d) and (e).

The Dirac surface state in $Bi_2Te_3(111)$ is strongly localized within the topmost quintuple layer (bottom row in Fig. 5), in agreement with earlier calculations. This state shows significant spectral weight (large color saturation) only in the first quintuple layer (f) but almost zero spectral weight in the deeper layers [(g)–(j)]. The layers chosen for panels [(a)–(e)], for SnTe(111), have almost the same distance from the surface atomic layer as the central atomic layers of the quintuple layers of Bi_2Te_3; this facilitates comparing the decay of the surface states in both compounds.

For the interface system SnTe(111)/Bi_2Te_3(111) (see Fig. 6, $\kappa = 1$), the Dirac state with Dirac point at $\overline{M}$, which is derived from the surface state in SnTe(111), survives, while the other two surface states annihilate. Its weak localization at the SnTe(111) surface (top row in Fig. 5) is also seen in the Bi_2Te_3 half-space; more precisely, it shows weak but nonzero spectral weight in the deeper layers, for example in (d) and in (i).

The Dirac surface state of Bi_2Te_3 can be "buried," that is, it is shifted from the outermost into deeper quintuple layers, by surface modification.[18] Attaching a SnTe half-space to the surface of Bi_2Te_3 may be viewed as a drastic surface alteration, which suggests a "burying" of the Dirac state. Inspection of Figs. 6(f)–6(j), however, shows no indication of a shift to deeper layers.

B. Interface electronic structure of Sb_2Te_3(111)/Bi_2Te_3(111)

For comparison with SnTe(111)/Bi_2Te_3(111), we calculated the electronic structure and its evolution with κ for Sb_2Te_3(111)/Bi_2Te_3(111). Since both subsystems belong to the same class of topological insulators—both their $\mathcal{Z}_2$ invariants and mirror Chern numbers are identical—the Dirac surface states of the uncoupled systems annihilate upon contact.

For the uncoupled subsystems, we find the established Dirac surface states of $Sb_2Te_3(111)$ and $Bi_2Te_3(111)$ with their Dirac points at $\overline{\Gamma}$ [$\kappa = 0$, panels (a) and (e) in Fig. 7]. Increasing the coupling strength κ opens up band gaps at the Dirac points [(b) and (f)], whose widths increase with κ [e. g., (c) and (g)]. In other words, the lower and the upper part of the Dirac

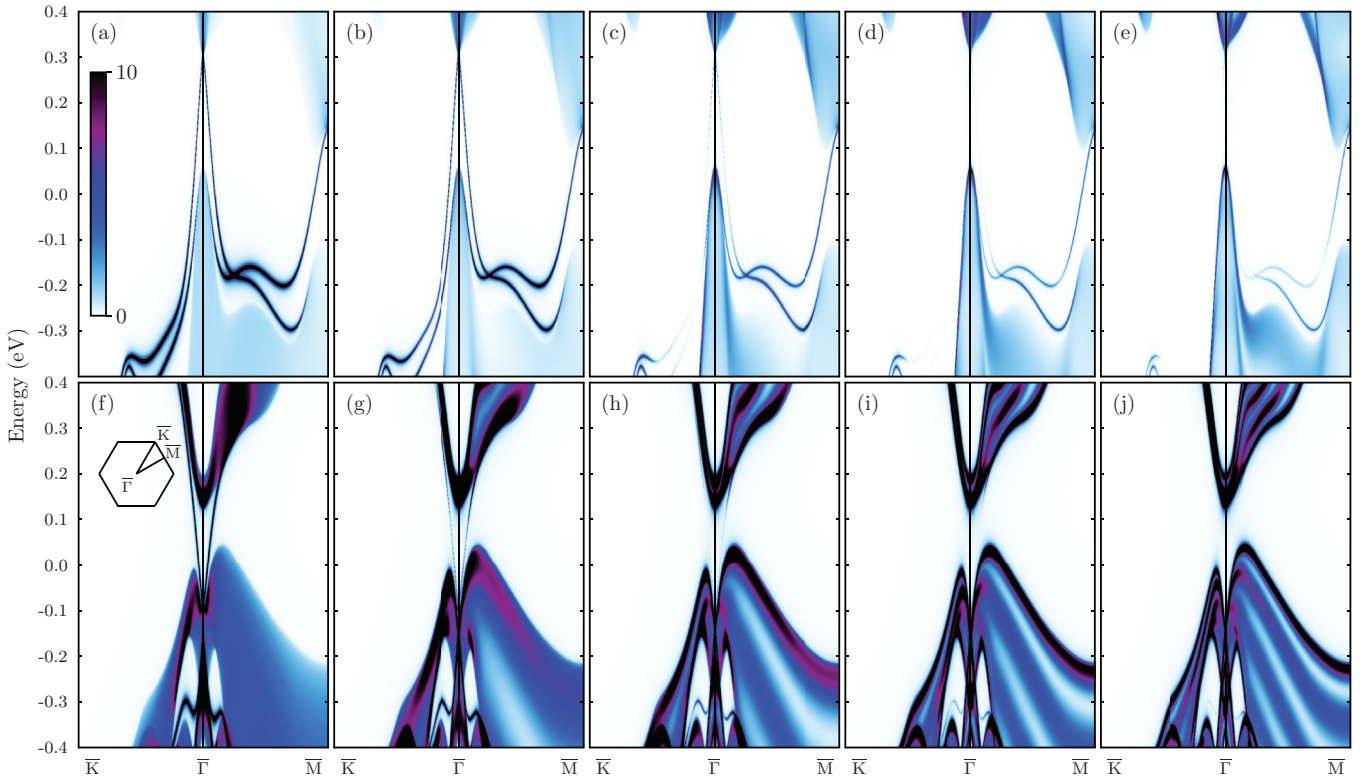

FIG. 5. (Color online) Localization of the surface states of SnTe(111) [top row, (a)–(e)] and Bi_2Te_3(111) [bottom row, (f)–(j)] for $\kappa = 0$ (i. e., uncoupled semi-infinite subsystems). For SnTe, spectral densities are shown for the second (a), the fourth (b), the seventh (c), the ninth (d), and the twelfth (e) double layer, counted from the surface. For Bi_2Te_3, spectral densities are shown for the first five quintuple layers, counted from the surface (f). The color scale in (a) gives the spectral density in states per eV; the two-dimensional Brillouin zone is sketched in (f).

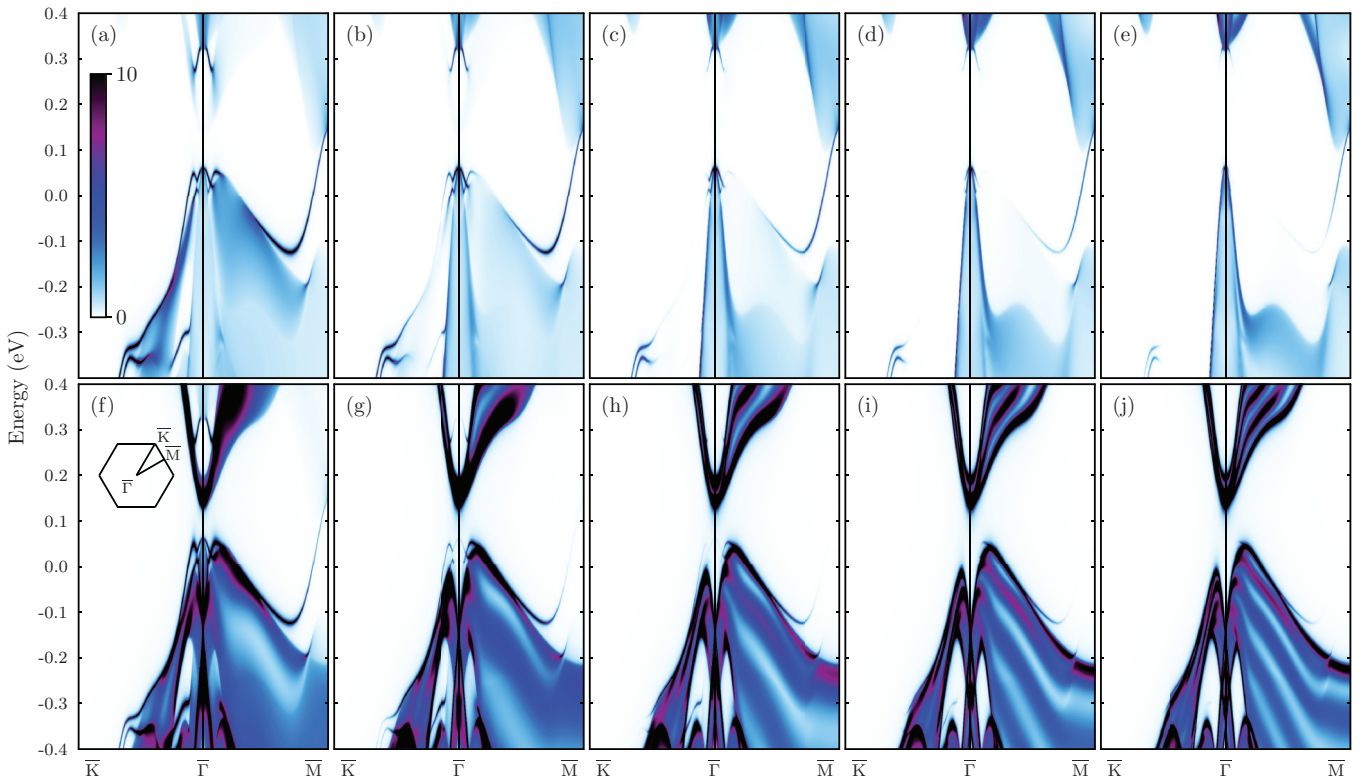

FIG. 6. (Color online) Localization of interface states of SnTe(111)/Bi_2Te_3(111) for $\kappa = 1$ (i. e., fully coupled semi-infinite subsystems). Panels and insets as in Fig. 5.

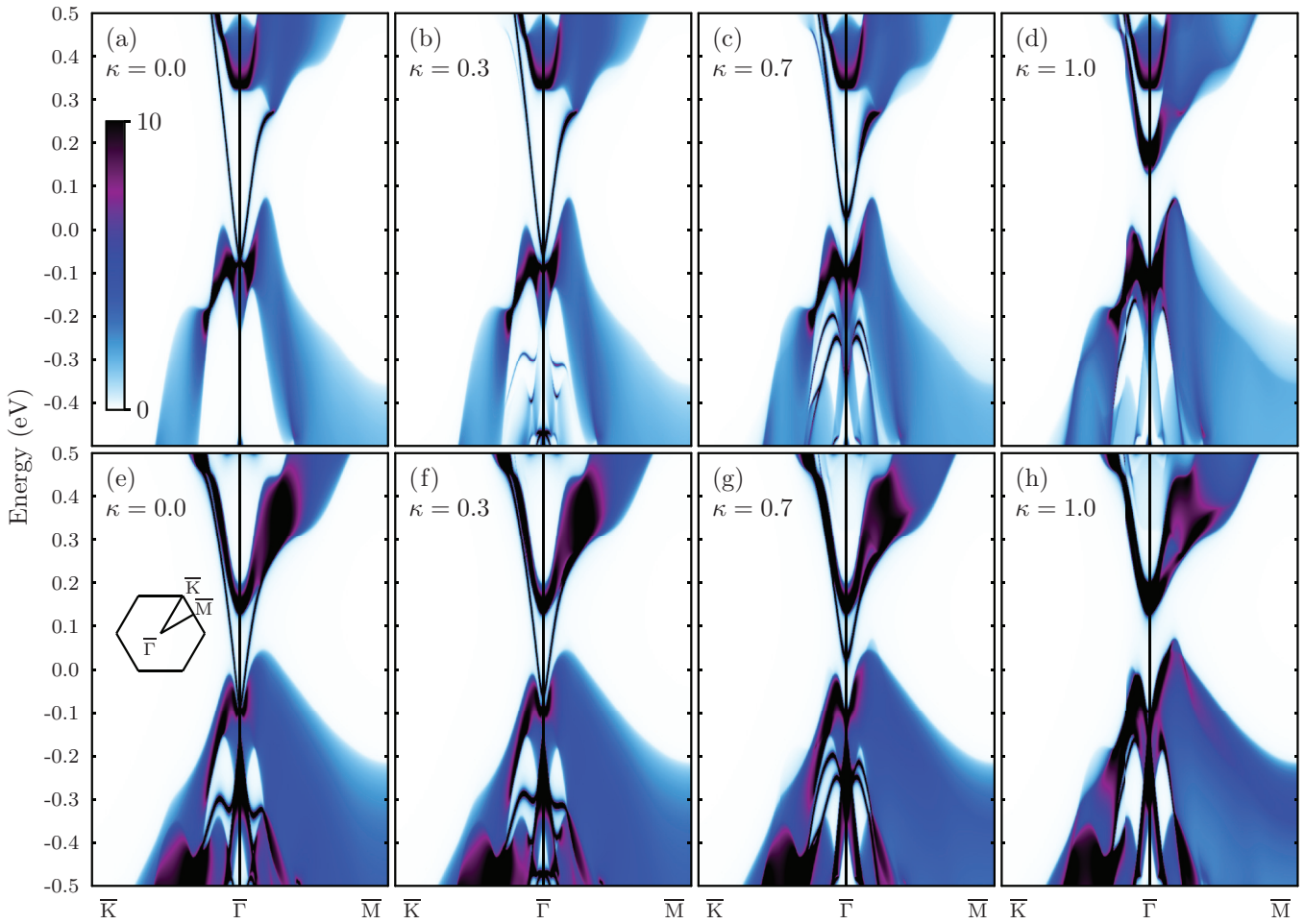

FIG. 7. (Color online) Interface electronic structure of $Sb_2Te_3(111)/Bi_2Te_3(111)$. Spectral densities of the outermost quintuple layers of Sb_2Te_3 [top row, (a)–(d)] and Bi_2Te_3 [bottom row, (e)–(h)] are shown for selected coupling strength κ, as indicated in each panel ($\kappa = 0$ for no coupling, i. e., separate surfaces; $\kappa = 1$ for fully coupled subsystems). The color scale in (a) gives the spectral density in states per eV; the two-dimensional Brillouin zone is sketched in (e).

cones detach; the lower part is shifted towards the valence bands while the upper part is shifted towards the conduction bands. For full coupling, $\kappa = 1$, the Dirac states are completely removed from the fundamental band gaps and merge with the bulk states, making the entire system insulating.

C. Sum rule for the Dirac states

The annihilation and survival of the Dirac states at a common interface with preserved mirror symmetry can be understood by means of a sum rule for the associated mirror Chern numbers.[7] For Bi_2Te_3 and SnTe, the Bloch states with mirror eigenvalue $+i$ possess the Chern numbers $n_{+i}^{BiTe} = -1$ and $n_{+i}^{SnTe} = -2$, respectively. At the common interface, $n_{+i}^{SnTe} - n_{+i}^{BiTe} = -1$ holds, which indicates that one interface state with eigenvalue $+i$ survives. The same rule applies for the Bloch states with eigenvalue $-i$; thus, there exists one topologically protected interface state with this mirror eigenvalue, too.

Concerning Sb_2Te_3 and Bi_2Te_3, $n_{\pm i}^{SbTe} = n_{\pm i}^{BiTe} = \mp 1$ holds because both subsystems show identical mirror Chern numbers. For the interface, this leads to $n_{\pm i}^{BiTe} - n_{\pm i}^{SbTe} = 0$ which implies that Dirac states do not "survive," in agreement with the electronic-structure calculations (Fig. 7).

IV. CONCLUDING REMARKS

The Dirac surface states of $\mathcal{Z}_2$ topological insulators are protected by time-reversal symmetry which makes them robust against structural disorder. In the present study, the remaining Dirac interface state is topologically protected by mirror symmetry because it is derived from the topological crystalline insulator SnTe. Hence, structural disorder which breaks the reflection symmetry would lead to opening of a band gap at the Dirac point. Since the Dirac point lies within the conduction bands, in-plane transport would be marginally affected by this band gap. Hence, a Bi_2Te_3/SnTe(111) interface is expected suitable for future electronic applications. In a recent transport experiment on a $SnTe/Bi_2Te_3(111)$ *pn* junction,[26] a signature of a conducting interface channel has not been found, which is attributed to electric decoupling of the subsystems due to doping.

To experimentally prove our theoretical findings, one could think of a film geometry investigated by angle-resolved

photoelectron spectroscopy in the soft x-ray regime.[42] This range of photon energies overcomes the too small electron mean free path in the vacuum ultraviolet range[43] and the too small photoionization cross sections in the hard x-ray regime, thus allowing Fermi surface mapping at the buried interface. Depth selectivity could be achieved by soft x-ray standing wave spectroscopy, e. g., Refs. 44 and 45. Considering spin-dependent transport, the interface state could be proven in $(SnTe/Bi_2Te_3)_n$ heterostructures: the conductance parallel to the interfaces increases with the number of interfaces in steps of the conductance quantum. The spin polarization could be probed by the inverse spin Hall effect.[46]

ACKNOWLEDGMENTS

We thank Silvia Picozzi and her group for fruitful discussions. This work is supported by the SPP 1666 "Topological Insulators" of DFG.

[1] H. Hasan and C. Kane, Rev. Mod. Phys. **82**, 3045 (2010).
[2] L. Fu, Phys. Rev. Lett. **106**, 106802 (2011).
[3] J. E. Moore and L. Balents, Phys. Rev. B **75**, 121306(R) (2007).
[4] J. C. Y. Teo, L. Fu, and C. L. Kane, Phys. Rev. B **78**, 045426 (2008).
[5] W. Zhang, R. Yu, H.-J. Zhang, X. Dai, and Z. Fang, New J. Phys. **12**, 065013 (2010).
[6] S. R. Park, J. Han, C. Kim, Y. Y. Koh, C. Kim, H. Lee, H. J. Choi, J. H. Han, K. D. Lee, N. J. Hur *et al.*, Phys. Rev. Lett. **108**, 046805 (2012).
[7] R. Takahashi and S. Murakami, Phys. Rev. Lett. **107**, 166805 (2011).
[8] T. H. Hsieh, H. Lin, J. Liu, W. Duan, A. Bansil, and L. Fu, Nat. Commun. **3**, 982 (2012).
[9] Y. Tanaka, Z. Ren, K. Nakayama, S. Souma, T. Takahashi, K. Segawa, and Y. Ando, Nat. Phys. **8**, 800 (2012).
[10] T. Rauch, M. Flieger, J. Henk, I. Mertig, and A. Ernst, Phys. Rev. Lett. (to be published).
[11] P. Barone, T. Rauch, D. Di Sante, J. Henk, I. Mertig, and S. Picozzi, Phys. Rev. B **88**, 045207 (2013).
[12] P. Pecheur and G. Toussaint, J. Phys. Chem. Solids **55**, 327 (1994).
[13] C. S. Lent, M. A. Bowen, J. D. Dow, and R. S. Allgaier, Superlatt. Microstruct. **2**, 491 (1986).
[14] N. Metropolis, A. W. Rosenbluth, M. N. Rosenbluth, and E. Teller, J. Chem. Phys. **21**, 1087 (1953).
[15] K. Binder and D. W. Heermann, *Monte Carlo Simulation in Statistical Physics: An Introduction*, 3rd ed. (Springer, Berlin, 1997).
[16] M. D. Jaffe and J. Singh, Sol. State Commun. **62**, 339 (1987).
[17] D. A. Papaconstantopoulos and M. J. Mehl, J. Phys.: Condens. Matter **15**, R413 (2003).
[18] S. V. Eremeev, G. Landolt, T. V. Menshchikova, B. Slomski, Y. M. Koroteev, Z. S. Aliev, D. M. Babanly, J. Henk, A. Ernst, L. Patthey *et al.*, Nature Commun. **3**, 635 (2012).
[19] J. Henk, A. Ernst, S. V. Eremeev, E. V. Chulkov, I. V. Maznichenko, and I. Mertig, Phys. Rev. Lett. **108**, 206801 (2012).
[20] J. Henk, M. Flieger, I. V. Maznichenko, I. Mertig, A. Ernst, S. V. Eremeev, and E. V. Chulkov, Phys. Rev. Lett. **109**, 076801 (2012).
[21] M. P. Lopéz Sancho, J. M. L. Sancho, and J. Rubio, J. Phys. F: Met. Phys. **15**, 851 (1985).
[22] J. Henk and W. Schattke, Comput. Phys. Commun. **77**, 69 (1993).
[23] A. Bödicker, W. Schattke, J. Henk, and R. Feder, J. Phys.: Condens. Matter **6**, 1927 (1994).
[24] R. Feder and K. Sturm, Phys. Rev. B **12**, 537 (1975).
[25] W. Harrison, *Electronic Structure and the Properties of Solids* (W. H. Freeman, San Francisco, 1980).
[26] A. A. Taskin, S. Sasaki, K. Segawa, and Y. Ando, arXiv:1305.2470 [cond-mat.mes-hall].
[27] J. Pollmann and S. T. Pantelides, Phys. Rev. B **18**, 5524 (1978).
[28] H. M. Benia, A. Yaresko, A. P. Schnyder, J. Henk, C. T. Lin, K. Kern, and C. R. Ast, Phys. Rev. B **88**, 081103 (2013).
[29] J. McCaldin, T. McGill, and C. Mead, Phys. Rev. Lett. **36**, 56 (1976).
[30] W. R. Frensley and H. Kroemer, Phys. Rev. B **16**, 2642 (1977).
[31] S. P. Kowalczyk, W. J. Schaffer, E. A. Kraut, and R. W. Grant, J. Vac. Sci. Tech. **20**, 705 (1982).
[32] L. Fu and C. L. Kane, Phys. Rev. B **74**, 195312 (2006).
[33] T. Fukui and Y. Hatsugai, J. Phys. Soc. Jpn. **76**, 053702 (2007).
[34] E. Prodan, Phys. Rev. B **80**, 125327 (2009).
[35] T. Inui, Y. Tanabe, and Y. Onodera, *Group Theory and Its Applications in Physics*, Springer Series in Solid State Sciences Vol. 78 (Springer, Berlin, 1990).
[36] L. Fu, Phys. Rev. Lett. **103**, 266801 (2009).
[37] F. Reinert, J. Phys.: Condens. Matter **15**, S693 (2003).
[38] C. R. Ast, J. Henk, A. Ernst, L. Moreschini, M. C. Falub, D. Pacilé, P. Bruno, K. Kern, and M. Grioni, Phys. Rev. Lett. **98**, 186807 (2007).
[39] M. König, S. Wiedmann, C. Brüne, A. Roth, H. Buhmann, L. W. Molenkamp, X.-L. Qi, and S.-C. Zhang, Science **318**, 766 (2007).
[40] O. V. Yazyev, J. E. Moore, and S. G. Louie, Phys. Rev. Lett. **105**, 266806 (2010).
[41] E. Simon, A. Szilva, B. Ujfalussy, B. Lazarovits, G. Zarand, and L. Szunyogh, Phys. Rev. B **81**, 235438 (2010).
[42] G. Berner, M. Sing, H. Fujiwara, A. Yasui, Y. Saitoh, A. Yamasaki, Y. Nishitani, A. Sekiyama, N. Pavlenko, T. Kopp *et al.*, Phys. Rev. Lett. **110**, 247601 (2013).
[43] M. P. Seah and W. A. Dench, Surf. Interf. Anal. **1**, 2 (1979).
[44] S.-H. Yang, B. S. Mun, N. Mannella, S.-K. Kim, J. B. Kortright, J. Underwood, F. Salmassi, E. Arenholz, A. Young, Z. Hussain *et al.*, J. Phys.: Condens. Matter **14**, L407 (2002).
[45] A. X. Gray, J. Minár, L. Plucinski, M. Huijben, A. Bostwick, E. Rotenberg, S.-H. Yang, J. Braun, A. Winkelmann, G. Conti, D. Eiteneer, A. Rattanachata, A. A. Greer, J. Ciston, C. Ophus, G. Rijnders, D. H. A. Blank, D. Doennig, R. Pentcheva, J. B. Kortright, C. M. Schneider, H. Ebert, and C. S. Fadley, EuroPhys. Lett. **104**, 17004 (2013).
[46] K. Ando and E. Saitoh, Nat. Commun. **3**, 629 (2012).
[47] J. Liu, W. Duan, and L. Fu, arXiv:1304.0430 [cond-mat.mtrl-sci].
[48] We recall that a slab geometry results in band gaps that are brought about by quantization of the wave vector perpendicular to the layers

("quantum confinement"). These artificial gaps could falsify the topological character of the surface or interface states.

[49]Termination by Sn atoms instead of Te atoms shifts the Dirac points from the conduction band edge to the valence-band edge; our calculations for Sn-terminated SnTe(111) confirm the results presented in Fig. 2 of Ref.47.

[50]Due to spin-orbit coupling, the parity of the spatial part of a wave function and its spin polarization are entangled.[35]